Available online at www.sciencedirect.com
ScienceDirect
Trans. Nonferrous Met. Soc. China 30(2020) 657−667
Transactions of Nonferrous Metals Society of China
www.tnmsc.cn

Processing map and hot deformation behavior of Ta-particle reinforced TiAl composite

Cheng-hao YUAN, Bin LIU, Yu-xi LIU, Yong LIU

State Key Laboratory of Powder Metallurgy, Central South University, Changsha 410083, China

Received 4 August 2019; accepted 17 February 2020

Abstract: The hot deformation behavior of a Ta-particle reinforced TiAl composite was studied. Ti−48Al−2Cr−2Nb−0.2W(at.%)/20vol.%Ta metal matrix composite was fabricated by spark plasma sintering. The deformation behavior was investigated by hot compression tests at the temperature ranging from 1050 to 1200 °C and the strain rate ranging from 1×10^{-3} to 1 s^{-1}. The constitutive equation containing true strain variables was established. The values of activation energy Q under different strain degrees are between 240 and 280 kJ/mol, which are lower than that of pure TiAl. Based on dynamic material modeling, the processing maps at various strain degrees were established, and the optimized parameters for hot working are 1050−1100 °C and 0.005−0.01 s^{-1}. The microstructural evolution during deformation was characterized, which indicated that the dynamic recrystallization plays an important role in this process.
Key words: TiAl-based composite; flow behavior; processing map; dynamics recrystallization

1 Introduction

Titanium aluminides have attracted tremendous attention in aerospace due to their excellent properties, such as low density, high specific strength, excellent high-temperature creep resistance and oxidation resistance [1,2]. Unfortunately, the intrinsic brittleness and poor fracture toughness make titanium aluminides sensitive to cracks, which inevitably results in the low defect tolerance under service conditions [3,4]. Nevertheless, the light-weight related properties of titanium aluminides are more desirable than the inherent brittleness. Therefore, many studies have been conducted to improve the plasticity and fracture toughness of TiAl intermetallics [5,6]. VOJTĚCH et al [7,8] found that Nb can enhance the high-temperature performance of TiAl intermetallics. POPELA and VOJTĚCH [9] developed adherent and dense boride layers that had a highly positive effect on the surface mechanical properties of the TiAl-based intermetallics. Recently, TiAl metal matrix composites (MMC) have been extensively studied with second phases such as TiB_2, Nb, TiC and carbon fibre added to improve the mechanical properties [10].

In order to further improve the mechanical properties of TiAl, it is necessary to refine the grain size. Hot working is deemed as an effective way for grain refining [11,12]. Meanwhile, it is also an important step for manufacturing different-shaped parts. Since the hot deformation process does not involve a single parameter, such as temperature, pressure, and strain, it is difficult but important to determine the optimal deformation parameters. The processing maps are widely used and have been successfully applied in many materials, including TiAl. LI et al [13] studied the hot deformation behavior of Ti−45Al−8.0Nb−0.2B−0.2W−0.02Y (at.%) alloy and recommended 1250 °C and 1×10^{-3} s^{-1} as forging parameters. WANG et al [14]

Foundation item: Project (51625404) supported by the National Natural Science Foundation for Distinguished Young Scholar of China
Corresponding author: Yong LIU, Tel: +86-731-88836939, E-mail: yonliu@csu.edu.cn;
Bin LIU, Tel: +86-731-88877669, E-mail: binliu@csu.edu.cn
DOI: 10.1016/S1003-6326(20)65240-2

established the processing maps of a Ti−47Al−2Cr−2Nb−0.2W−0.15B (at.%) titanium aluminide alloy, and revealed the instability regions. BAO et al [15] calculated the activation energy of hot-isostatically-pressed Ti−47.5Al−2Cr−2Nb−0.2W−0.2B (at.%) alloy based on the constitutive relationship models developed with the Arrhenius-type constitutive model, and the value was approximately 365.5 kJ/mol.

Since Ta possesses very high melting point (3017 °C), low thermal expansion coefficient (6.5×10^{-3}) and excellent oxidation resistance [16], and can improve the high temperature performance of TiAl [7,8], it is selected as the second phase particle for TiAl matrix to form metal−metal matrix composite. In this study, the high-temperature compression behavior of a TiAl−20vol.%Ta metal matrix composite was investigated, and the processing maps under various true strains were established. The influence of deformation parameters on the microstructure evolution was also discussed.

2 Experimental

2.1 Materials preparation

TiAl−20vol.%Ta metal matrix composites were prepared by powder metallurgy method. Ti−48Al−2Cr−2Nb−0.2W pre-alloyed powder and pure Ta element powder were mixed in a V-type mixer for 12 h, and then were put into graphite mould. The powders were spark plasma sintered (SPS, FCT D25/3, FCT Systeme GmbH, Rauenstein, Germany) at 1400 °C and 30 MPa for 20 min under vacuum.

2.2 Hot compression

Cylindrical specimens, with a diameter of 8 mm and a height of 12 mm, were cut from the SPS-treated samples by electrical discharge machining. The hot compression tests were conducted on a Gleeble 3800 thermomechanical simulator at the temperature ranging from 1050 to 1200 °C in 50 °C interval and the strain rate ranging from 1×10^{-3} to 1 s^{-1}. A layer of tantalum sheet and graphite sheet were put on the two ends of the specimens to reduce friction. The temperature was measured by welding thermocouple wires around the sample. Specimens were heated with a heating rate of 10 °C/min from room temperature to 900 °C by induction coils firstly, and then with a heating rate of 5 °C/min from 900 °C to test temperatures. All the specimens were soaked at the test temperatures for 180 s before compression tests, and then deformed to half of their height, namely, 50% engineering strain. The whole process was in the protection of argon atmosphere. After compression, to preserve the high temperature deformation structure, the specimens were taken out and quenched in water immediately.

2.3 Characterization

The values of the density of composite samples were measured through Archimedes method. Microstructural observation before and after deformation was carried out by using scanning electron microscopy (SEM, Nova NanoSEM230, FEI, Hillsboro, OR, USA) using back scattering electron (BSE) imaging and the composition was detected by energy dispersive spectroscopy (EDS). Images were obtained from the cross-sectional surface cut parallel to the compression axis. The surface was ground by using emery paper, and polished by using OPS (Silica suspension) mixed with a small amount of hydrogen peroxide. X-ray diffraction (XRD, Max255Ovb+, RigakuD, Tokyo, Japan) analysis was conducted using Cu K_α radiation to examine the phase constitution and the scanning angle (2θ) ranged from 10° to 80° with a step size of 0.02°.

3 Results

3.1 Initial microstructures

Figure 1(a) shows the microstructure of the pre-alloyed TiAl powder with an average diameter of 200 μm. It can be seen that the powder particles are nearly spherical in shape. Combining the results of XRD (Fig. 1(b)), there are two main phases, γ-TiAl and α_2-Ti_3Al. Figure 1(c) shows the morphology of the Ta particle, and it appears in irregular shape. The XRD patterns of TiAl−20vol.%Ta composite is shown in Fig. 1(d). Besides the γ-TiAl, α_2-Ti_3Al and Ta phases existing in the original powder, $TaAl_3$ and β phases are also formed. The microstructure of the TiAl−20vol.%Ta metal matrix composites before the deformation is shown in Fig. 1(e), and three main types of contrast can be observed. Four small areas are selected and analyzed by EDS, and the results are listed in

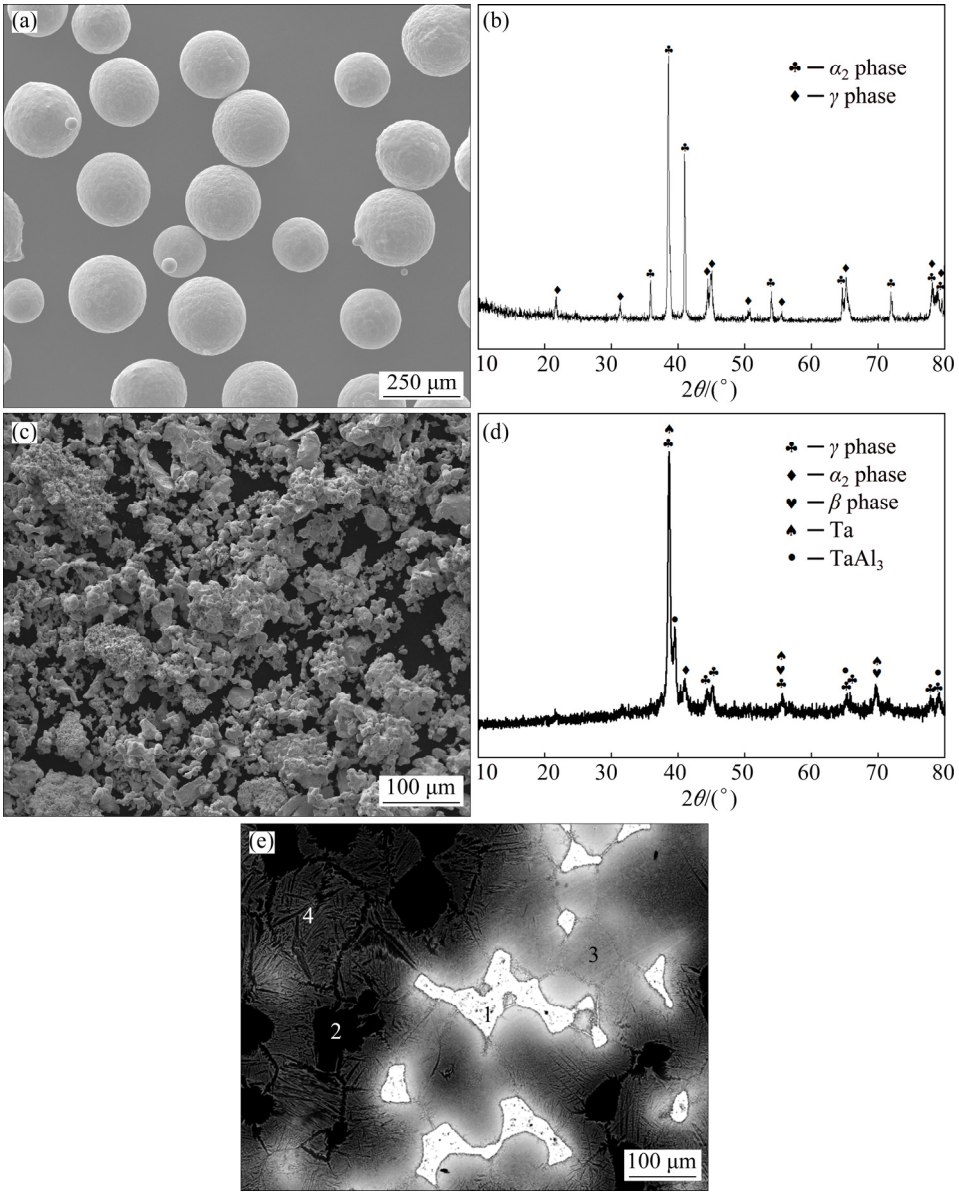

Fig. 1 Microstructures of powder and SPS-treated composite: (a) SEM image of TiAl powder; (b) XRD pattern of TiAl powder; (c) SEM image of Ta powder; (d) XRD pattern of TiAl−20vol.%Ta composite; (e) SEM image of TiAl−20vol.%Ta composite

Table 1. According to the XRD and EDS analyses, it can be found that Area 1 is pure Ta, Area 2 is pure TiAl, Area 3 and Area 4 are TiAl-rich phases containing 10−16 at.% Ta. Because the content of Ta in Area 3 is relatively high, it is shown that Area 4 contains lamellar structure and β phases. The average grain size of TiAl matrix is measured to be about 150 μm.

Table 1 EDS analysis results of four areas in Fig. 1(e) (at.%)

Area	Al	Ti	Ta	Nb	Cr	W
1	5.76	1.81	87.17	0.11	2.21	2.94
2	41.05	54.29	0.39	1.72	2.24	0.31
3	37.64	36.37	21.15	1.02	2.54	1.28
4	38.79	41.32	15.84	1.29	1.93	0.83

3.2 Deformation behavior

3.2.1 Flow behavior

The typical true stress−true strain curves of TiAl−20vol.%Ta composite obtained from the high-temperature compression tests are shown in Fig. 2. It is found that the flow stress is sensitive to the deformation temperature and the strain rate. With the increase of temperature and the decrease of strain rate, all the flow stresses decrease in a similar mode with the change of deformation condition. At

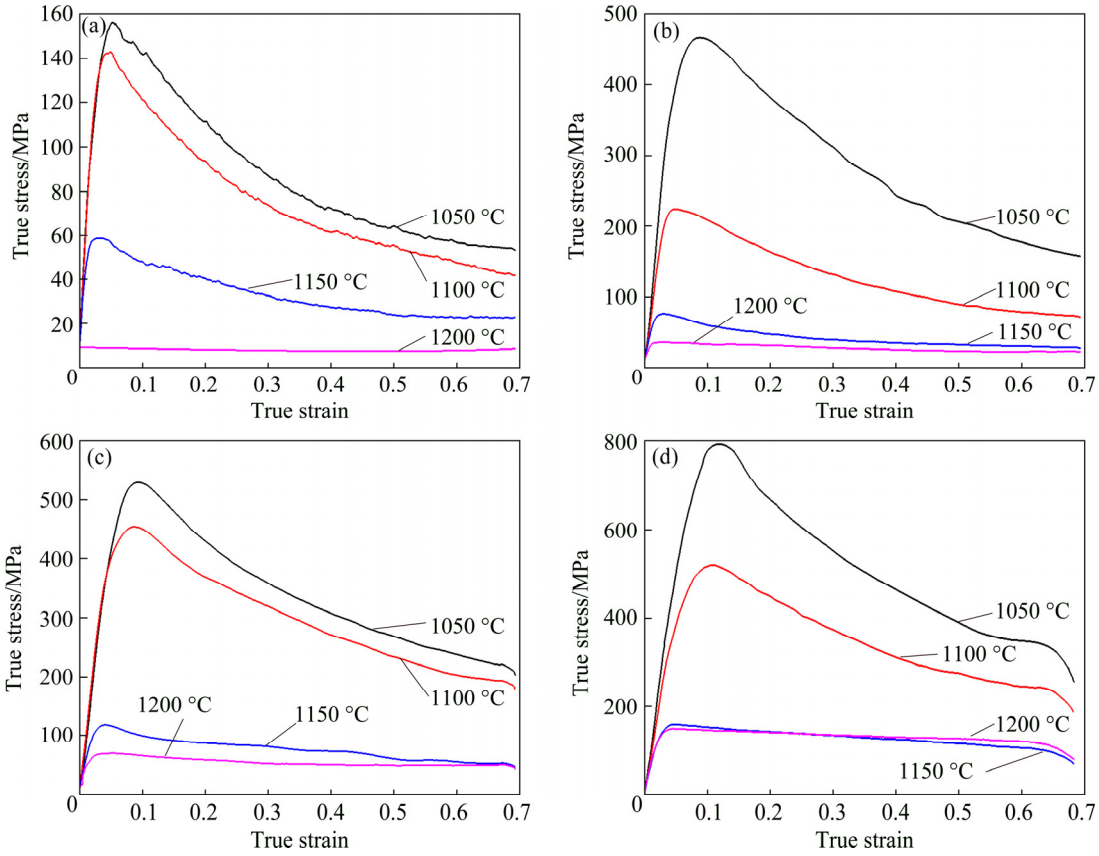

Fig. 2 True stress−true strain flow curves of TiAl−20vol.%Ta composite at at temperatures ranging from 1050 to 1200 °C with different strain rates: (a) 1×10^{-3} s^{-1}; (b) 1×10^{-2} s^{-1}; (c) 1×10^{-1} s^{-1}; (d) 1 s^{-1}

the initial stage of deformation, the flow stress increases linearly and rapidly with the increase of true strain, and quickly reaches the peak stress. After the peak stress, the flow stress decreases with the increase of true strain, indicating that the softening caused by the dynamic recrystallization (DRX) is greater than the hardening. In the final stage, the flow stress curve eventually becomes even at high strain.

3.2.2 Constitutive equation

The constitutive relationship among the flow stress, the strain rate and the deformation temperature during hot compression deformation can be described by the power-law relationship at low stress level and exponential relationship at high stress level:

At low stress level:

$$Z=\dot{\varepsilon}\exp[Q/(RT)]=A_1\sigma^{n_1} \quad (1)$$

At high stresses level:

$$Z=\dot{\varepsilon}\exp[Q/(RT)]=A_2\exp(\beta\sigma) \quad (2)$$

where Z is Zener−Hollomon parameter, Q is the deformation activation energy (kJ/mol), R is mole gas constant (8.314 $J\cdot mol^{-1}\cdot K^{-1}$), T is deformation temperature (K), and A_1, A_2, n_1 and β are material constants.

These two equations could be combined into a hyperbolic sine function:

$$Z=\dot{\varepsilon}\exp[Q/(RT)]=A[\sinh(\alpha\sigma)]^n \quad (3)$$

where A, α and n are material constants, and $\alpha=\beta/n_1$.

Since a true strain condition is determined, the slopes of $\ln\sigma-\ln\dot{\varepsilon}$ curve and $\sigma-\ln\dot{\varepsilon}$ curve can be obtained, namely, n_1 and β. Then, α can be calculated by β/n_1.

Equation (4) is equivalent to Eq. (3) through differential transformation on both sides of Eq. (3):

$$Q=R\left\{\frac{\partial\ln\dot{\varepsilon}}{\partial\ln[\sinh(\alpha\sigma)]}\right\}_T\left\{\frac{\partial\ln[\sinh(\alpha\sigma)]}{\partial(1/T)}\right\}_{\dot{\varepsilon}} \quad (4)$$

It can be seen that the Q value can be calculated by the slopes of $\ln\dot{\varepsilon}-\ln[\sinh(\alpha\sigma)]$ curve and $\ln[\sinh(\alpha\sigma)]-1/T$ curve.

Introducing the calculated Q value, the corresponding $\dot{\varepsilon}$ and T values into Eq. (3), the $\ln Z$ value under different deformation parameters

can be obtained.

By using the above method, the material constants under different true strain conditions can be calculated. Fitting these material constants by quintic function, the curves in Fig. 3 can be obtained. In Fig. 3(b), the activation energy is higher in the initial stage of deformation, which makes deformation more difficult, and thus only elastic−plastic deformation occurs. Then, the activation energy begins to decrease, indicating that the storage energy accumulated in the plastic deformation process starts to form DRX, gradually offsets the influence of work hardening and improves the deformation ability. And the activation energy fluctuates at a lower level, which is related to the alternation of softening caused by DRX and hardening caused by deformation. This is similar to the variation of flow stress.

Based on above, the constitutive equation of TiAl−20vol.%Ta composite containing true strain variables is as follows:

$$\sigma=\frac{1}{\alpha}\ln\left[\left(\frac{Z}{A}\right)^{1/n}+\left(\left(\frac{Z}{A}\right)^{2/n}+1\right)^{1/2}\right] \tag{5}$$

where

$$\begin{cases} Z=\dot{\varepsilon}\exp[Q/(RT)] \\ \alpha=0.3949\varepsilon^5-0.5266\varepsilon^4+0.2259\varepsilon^3- \\ \quad 0.0313\varepsilon^2+0.0092\varepsilon+0.0076 \\ Q=-47503\varepsilon^5+77649\varepsilon^4-47584\varepsilon^3+ \\ \quad 13713\varepsilon^2-1908.2\varepsilon+352.26 \\ \ln A=-4137.2\varepsilon^5+6729.1\varepsilon^4-4097\varepsilon^3+ \\ \quad 1171.2\varepsilon^2-161.07\varepsilon+26.054 \\ n=-184.67\varepsilon^5+319.68\varepsilon^4-206.67\varepsilon^3+ \\ \quad 62.764\varepsilon^2-9.2755\varepsilon+3.01 \end{cases}$$

3.2.3 Processing maps

The processing map is based on the principle of dynamic material modeling (DMM) [17], and it is very effective for determining optimum hot working parameters. In the process of processing, the external work putting on materials is mainly used for two aspects: one is the energy corresponding to plastic deformation, and the other is used for the evolution of microstructures, such as recovery, recrystallization, and phase transformation [18].

The power dissipation efficiency η is given by Eq. (6), and it is a ternary variable with temperature,

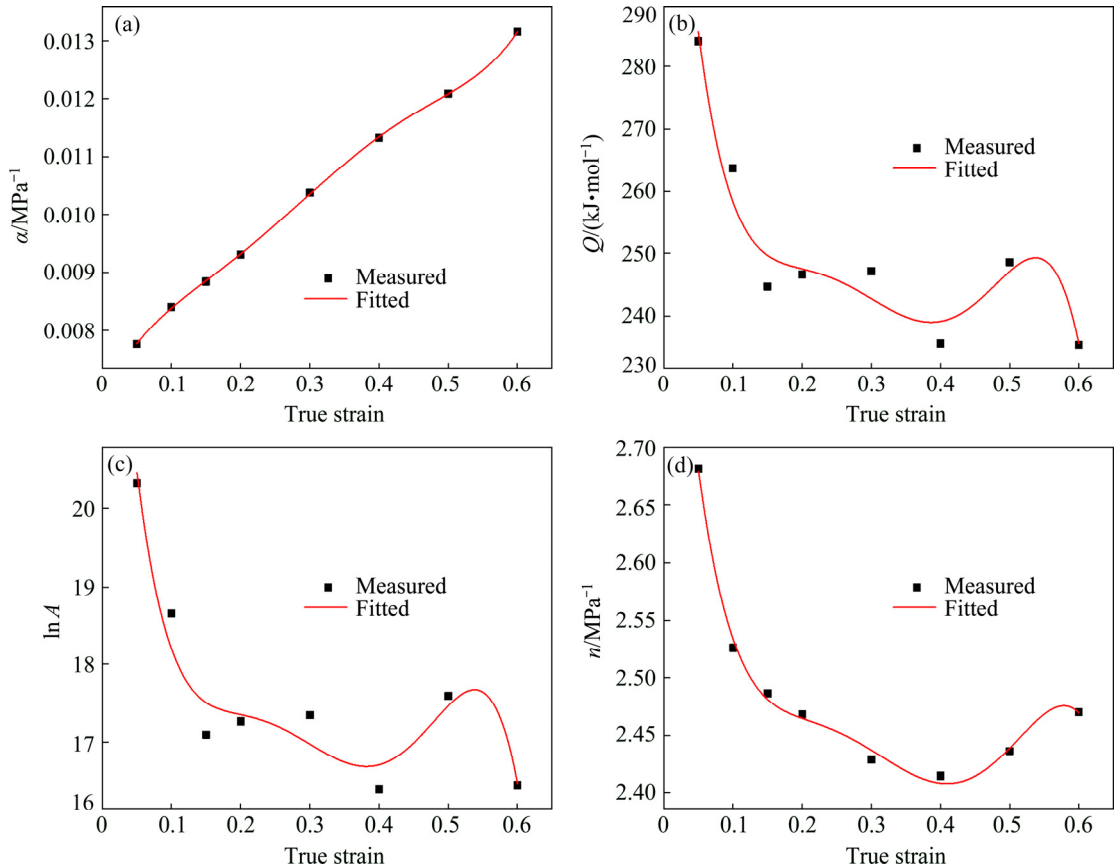

Fig. 3 Relationship between material constants and true strain by polynomial fit: (a) α; (b) Q; (c) ln A; (d) n

strain and strain rate. In theory, the greater the value of η is, the better the workability of the material is. Drawing the relationship among η, temperature and strain rate, the energy dissipation diagram can be obtained.

$$\eta = 2m/(m+1) \tag{6}$$

where m is strain rate sensitive factor and is equal to $\partial \ln\sigma / \partial \ln\dot{\varepsilon}$.

Since the value of η in the processing instability zone may also be high, it is necessary to determine the processing instability zone of material and use dimensionless parameters $\zeta(\dot{\varepsilon})$, defined by Eq. (7), as the criterion of continuous instability in plastic deformation. By labeling the region with negative values in the relation schema among $\zeta(\dot{\varepsilon})$, temperature and strain rate, the processing instability diagram can be obtained.

$$\xi(\dot{\varepsilon}) = \frac{\partial \ln[m/(m+1)]}{\partial \ln\dot{\varepsilon}} + m < 0 \tag{7}$$

By overlying the energy dissipation diagram and the processing instability diagram, the processing map can be obtained. Because TiAl-based alloys are prone to DRX during hot working, the effect of true strain must be taken into consideration.

Figure 4 shows the processing maps of the

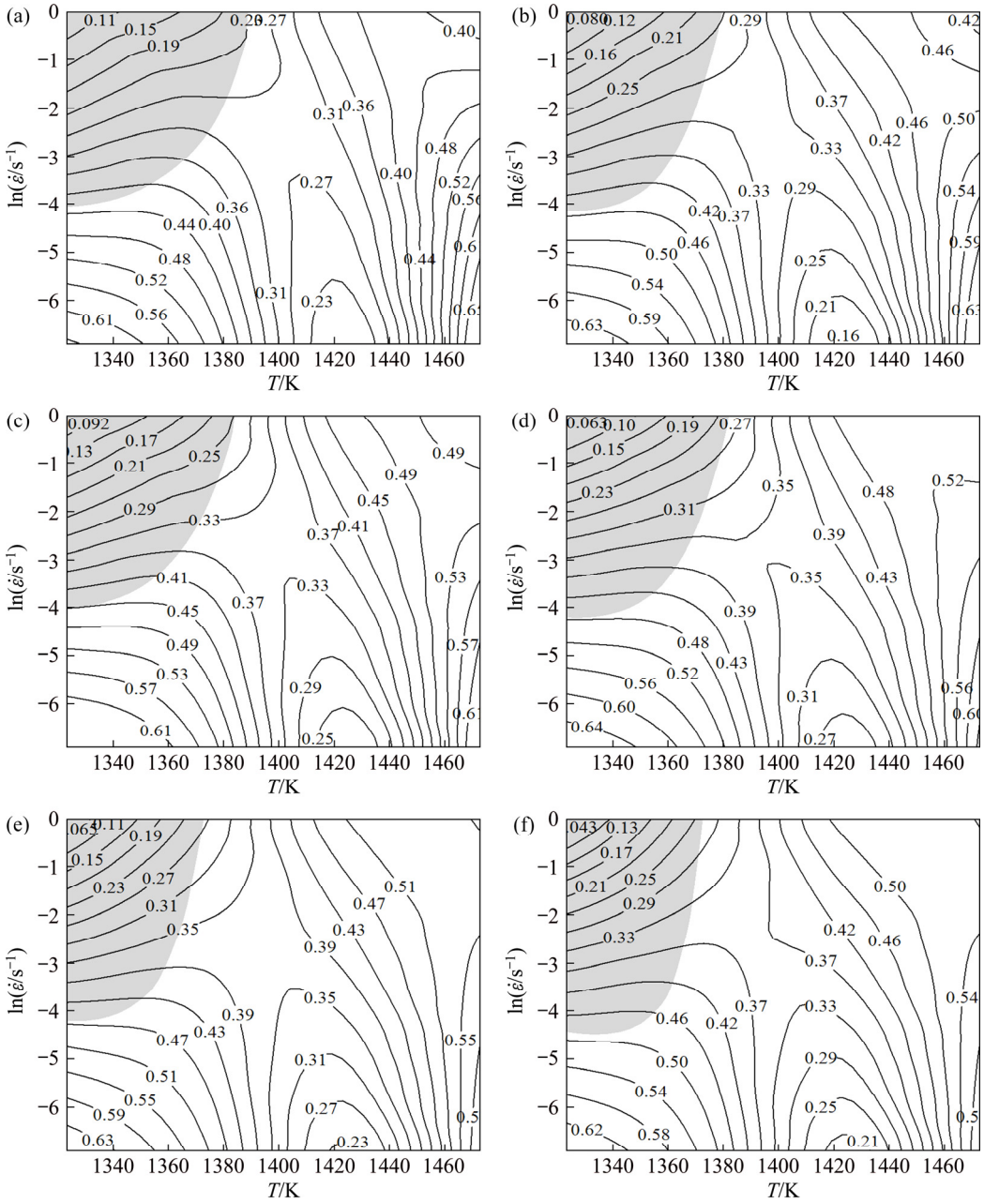

Fig. 4 Processing maps of TiAl−20vol%Ta composite at various true strains: (a) 0.1; (b) 0.2; (c) 0.3; (d) 0.4; (e) 0.5; (f) 0.6

composite at various true strains. It is found that the instability zone (gray shadow) varies with the increase of strain, it becomes narrow with the decrease of temperature, and becomes wide with the decrease of strain rate, but the overall change is not obvious. For each strain condition, all the instability zones correspond to the low temperature and high strain rate area, and the η values in these regions are low, ranging from 0.10 to 0.30, indicating that it is not easy to process the material. At temperatures ranging from 1330 to 1380 K and $\ln\dot{\varepsilon}$ ranging from −6.5 to −4.5, the η values increase to 0.50−0.63. High η value means good workability and even superplasticity. At temperatures higher than 1450 K, the η values are greater than 0.45 in almost all strain rate ranges. However, the contours of power dissipation efficiency in these regions are narrow, and a slight variation of deformation parameters in these regions may induce unstable deformation. Considering that the slow strain rate needs long processing time, the processing parameters are recommended to be 1050−1100 °C and 0.005−0.01 s^{-1}.

3.3 Deformation microstructures

Figure 5 shows the microstructures of the materials deformed under different conditions. Figures 5(a) and (b) show the microstructures deformed at different temperatures with a strain rate of 1×10^{-2} s^{-1}. At 1050 °C, the microstructures are mostly unrecrystallized, and the lamellar structures still exist (Fig. 5(a)). At 1200 °C, DRX occurs in a large number of lamellar structures, and the DRX grains (marked as "*A*") appear around the unrecrystallized regions (marked as "*B*"). The microstructures of samples compressed at 1100 °C and different strain rates are shown in Figs. 5(c) and 5(d). It can be seen that the degree of DRX does not obviously change with the change of the strain rate at the same temperature. That is to say, the effect of the strain rate on the microstructure is not as obvious as that of the deformation temperature.

The SEM images in Fig. 6 exhibit the microstructures in the regions with low η values (1100 °C, 0.1 s^{-1}) and high η values (1050 °C, 0.001 s^{-1}). The lamellar bending can be found in the lower left corner of Fig. 6(a). It has been

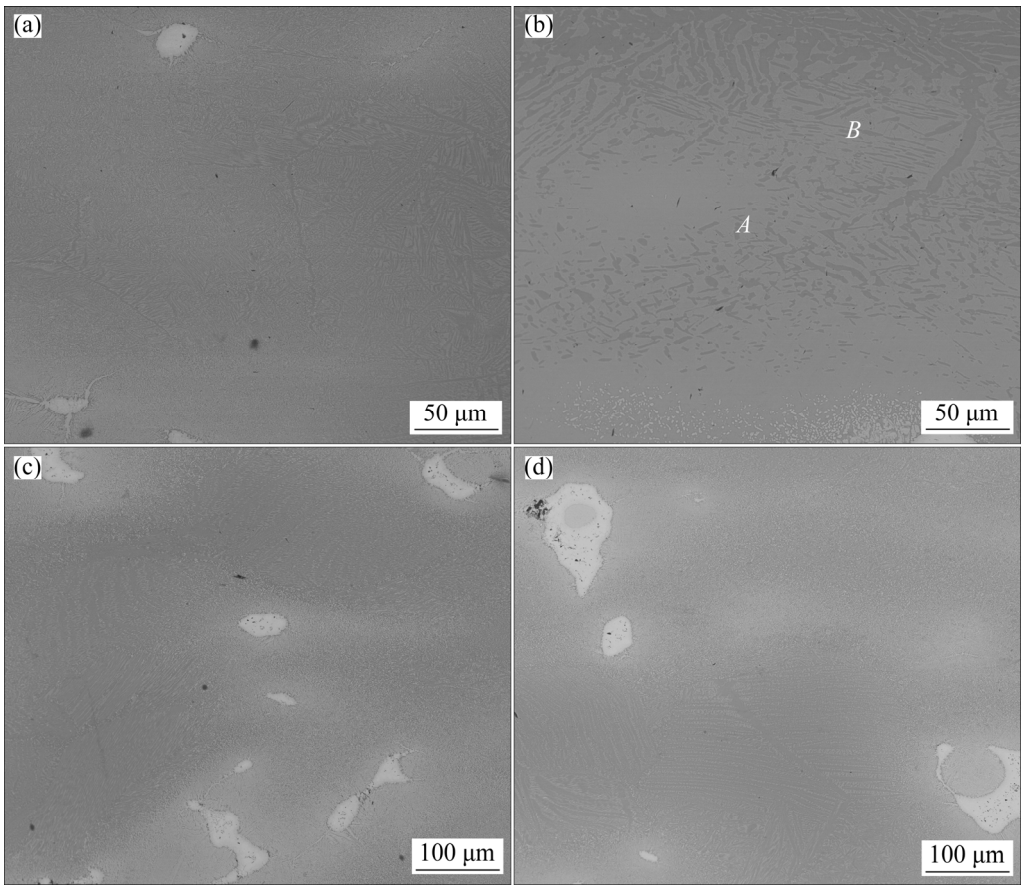

Fig. 5 Microstructures of TiAl−20vol.%Ta composite deformed under different deformation conditions: (a) 1050 °C, 1×10^{-2} s^{-1}; (b) 1200 °C, 1×10^{-2} s^{-1}; (c) 1100 °C, 1×10^{-3} s^{-1}; (d) 1100 °C, 1×10^{-2} s^{-1}

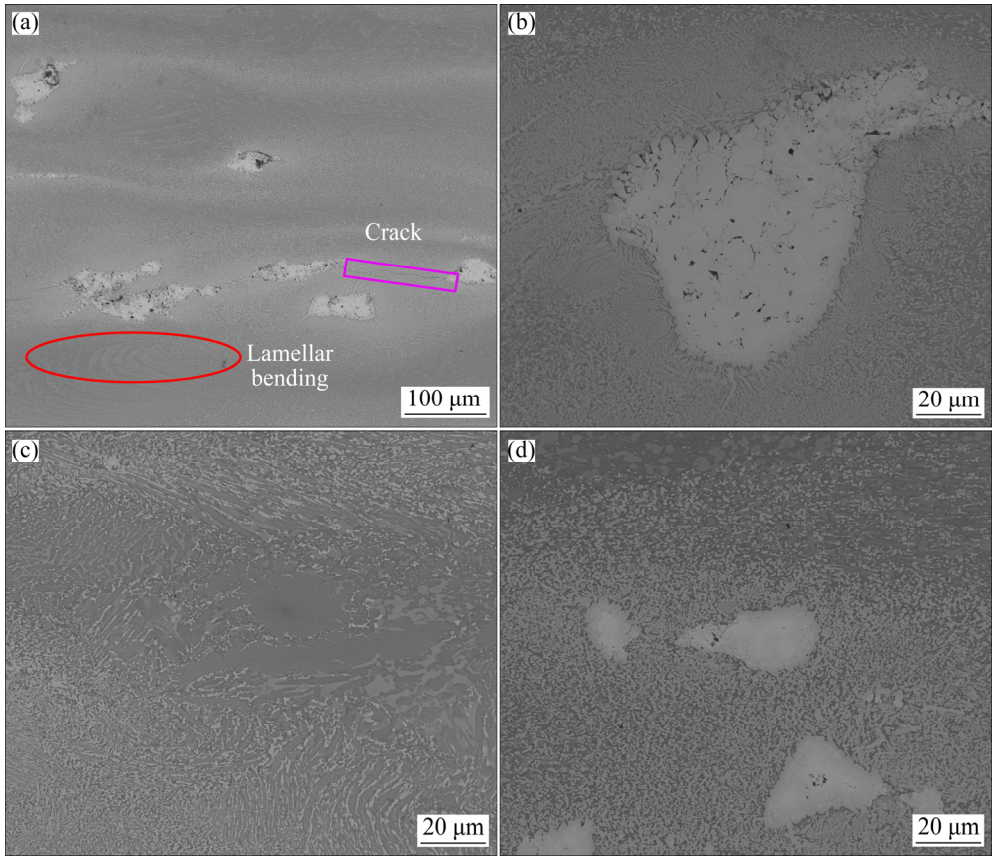

Fig. 6 Microstructures of different regions in TiAl−20vol.%Ta composite deformed at different η values: (a) 1100 °C, 1×10^{-1} s^{-1}, overall area; (b) 1100 °C, 1×10^{-1} s^{-1}, Ta-rich area; (c) 1050 °C, 1×10^{-3} s^{-1}, TiAl-rich area; (d) 1050 °C, 1×10^{-3} s^{-1}, Ta-rich area

reported that grains can be elongated and the lamellar structure decreases after hot deformation, the layered structures in the direction perpendicular to the compression direction will be stretched and those parallel to the compression direction will be bent [19]. Cracks and pores can also be observed in Figs. 6(a) and (b), and it is found that the defects mainly distribute in Ta-rich area. In contrast, the defects in Figs. 6(c) and (d) are significantly reduced. The defects are almost not found in TiAl-rich area, and only several tiny pores can be observed in Ta-rich area. This proves that Ta undertakes the main plastic deformation in the compression process, leading to higher η value and better processability.

Figure 7 shows the microstructures deformed in instable (1050 °C, 1 s^{-1}) and stable (1150 °C, 1×10^{-1} s^{-1}) zones. It is easy to find that extensive micropores distribute in TiAl-rich area, especially in lamellar structures. Unlike Fig. 6(b), only a few pores or cracks are found in Fig. 7(b) owing to the stress relaxation of Ta-rich particles. Figures 7(c) and 7(d) are similar to Figs. 6(c) and 6(d). Therefore, the composite possesses good workability under this deformation condition, with a steady-state flow behavior.

4 Discussion

Table 2 shows Q values and unstable regions of TiAl and composites with different compositions. It can be seen that the deformation activation energy of TiAl−20vol.%Ta composite is significantly lower than those of other TiAl, and the instable regions in this work is obviously smaller.

The reasons can be explained from the following three aspects. (1) Ta particles have a lower critical resolved shear stress (CRSS) than TiAl matrix. The CRSS for single crystal Ta is only 5 kg/mm^2 (50 MPa) at room temperature [25], while the CRSS for single crystal TiAl can still reach 120 MPa beyond 1000 K [26]. With the increase of temperature, the material will soften, so the CRSS of Ta at high temperatures is much less

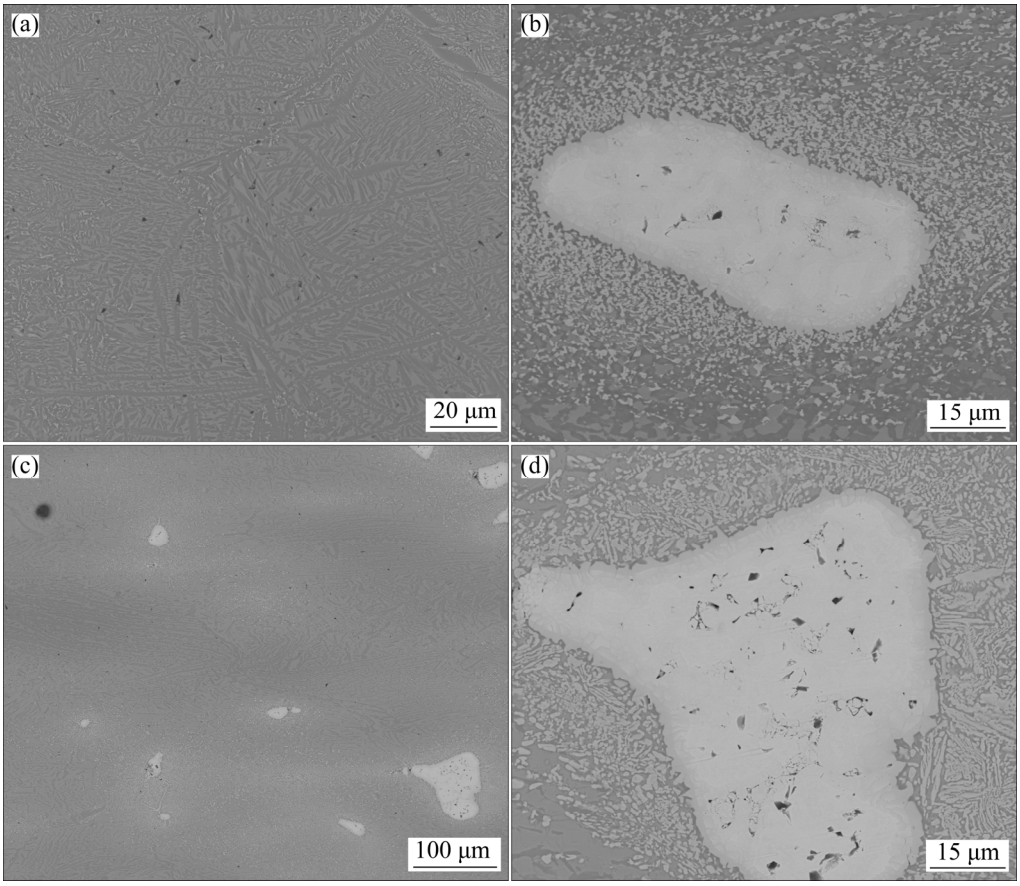

Fig. 7 Microstructures of different regions in TiAl−20vol.%Ta composite deformed in unstable and stability zones: (a) 1050 °C, 1 s^{-1}, TiAl-rich area; (b) 1050 °C, 1 s^{-1}, Ta-rich area; (c) 1150 °C, 1×10^{-1} s^{-1}, overall area; (d) 1150 °C, 1×10^{-1} s^{-1}, Ta-rich area

Table 2 Q values and instable regions of TiAl and composites with different compositions

Alloy	Q/(kJ·mol^{-1})	Unstable region
TiAl−20vol.%Ta	240−280	1320−1380 K, 0.01−1 s^{-1}
PM Ti−47Al−2Cr−2Nb−0.2W−0.15B [14]	360	1220−1573 K, 0.9−10 s^{-1}
Ti–43Al–4Nb–1.4W–0.6B [20]	580.68	−
Ti−45Al−5Nb−0.4W/2Nb [21]	450−620	−
As-cast Ti−43Al−4Nb−1.4W−0.6B [22]	419	1320−1370 K, 0.04−1 s^{-1}; 1400−1480 K, 0.06−1 s^{-1}
PM Ti–47Al–2Nb–2Cr [23]	356	1223−1473 K, 0.02−0.1 s^{-1}
As-cast Ti−45Al−8Nb−2Cr−0.2B [24]	−	1273−1473 K, 0.1−1 s^{-1}

than that of TiAl. Low CRSS means low stress required for deformation, and consequently leads to a decrease in activation energy. (2) Ta is a β stabilizing element for Ti and TiAl [27], and it can introduce the formation of β phase in TiAl. The β phase is expected to be softer than α_2 and γ phases during hot deformation due to its disordered lattice [28] and more independent slip systems. (3) In Figs. 6 and 7, a large number of fine-grained structures can be observed around the Ta-rich area due to the inter diffusion of Ta with TiAl matrix. The fine structures have good plasticity and can coordinate the deformation between the TiAl-rich area and the Ta-rich area. Therefore, the stable deformation region of the composite is larger than that of other TiAl.

5 Conclusions

(1) The flow stress PM TiAl−20vol.%Ta composite decreases with the increase of temperature and the decrease of strain rate.

(2) Under different strain conditions, the activation energy of the composite is lower than that of other TiAl alloys, which indicates that the addition of plastic element Ta particles makes the deformation of titanium aluminides easier.

(3) The addition of Ta particle is responsible for the wider stable region in the processing maps of TiAl−20vol.%Ta composite than other TiAl alloys.

(4) Considering the distribution of unstable zone, the recommended processing parameters for TiAl−20vol.%Ta composite are as follows: 1050−1100 °C and 0.005−0.01 s^{-1}.

References

[1] KENEL C, DASARGYRI G, BAUER T, COLELLA A, SPIERINGS A B, LEINENBACH C, WEGENER K. Selective laser melting of an oxide dispersion strengthened (ODS) γ-TiAl alloy towards production of complex structures [J]. Materials & Design, 2017, 134: 81−90.

[2] CHLUPOVÁ A, HECZKO M, OBRTLÍK K, POLÁK J, ROUPCOVÁ P, BERAN P, KRUML T. Mechanical properties of high niobium TiAl alloys doped with Mo and C [J]. Materials & Design, 2016, 99: 284−292.

[3] DING Hong-sheng, NIE Ge, CHEN Rui-run, GUO Jing-jie, FU Heng-zhi. Influence of oxygen on microstructure and mechanical properties of directionally solidified Ti−47Al−2Cr−2Nb alloy [J]. Materials & Design, 2012, 41: 108−113.

[4] ERDELY P, STARON P, MAAWAD E, SCHELL N, KLOSE J, MAYER S, CLEMENS H. Effect of hot rolling and primary annealing on the microstructure and texture of a β-stabilised γ-TiAl based alloy [J]. Acta Materialia, 2017, 126: 145−153.

[5] VOISIN T, MONCHOUX J P, HANTCHERLI M, MAYER S, CLEMENS H, COURET A. Microstructures and mechanical properties of a multi-phase β-solidifying TiAl alloy densified by spark plasma sintering [J]. Acta Materialia, 2014, 73: 107−115.

[6] LAPIN J, ŠTAMBORSKÁ M, PELACHOVÁ T, BAJANA O. Fracture behaviour of cast in-situ TiAl matrix composite reinforced with carbide particles [J]. Materials Science & Engineering A, 2018, 721: 1−7.

[7] VOJTĚCH D, POPELA T, HAMÁČEK J, KÜTZENDÖRFERB J. The influence of tantalum on the high temperature characteristics of lamellar gamma + alpha 2 titanium aluminide [J]. Materials Science & Engineering A, 2011, 528: 8557−8564.

[8] VOJTĚCH D, POPELA T, KUBÁSEK J, MAIXNER J, Novák P. Comparison of Nb- and Ta-effectiveness for improvement of the cyclic oxidation resistance of TiAl-based intermetallics [J]. Intermetallics, 2011, 19: 493−501.

[9] POPELA T, VOJTĚCH D. Characterization of pack-borided last-generation TiAl intermetallics [J]. Surface & Coatings Technology, 2012, 209: 90−96.

[10] LI Wei, YANG Yi, LI Ming, LIU Jie, CAI Dao-sheng, WEI Qing-song, YAN Chun-ze, SHI Yu-sheng. Enhanced mechanical property with refined microstructure of a novel γ-TiAl/TiB_2 metal matrix composite (MMC) processed via hot isostatic press [J]. Materials & Design, 2018, 141: 57−66.

[11] LIU Bin, LIU Yong, ZHANG Wei, HUANG Jin-song. Hot deformation behavior of TiAl alloys prepared by blended elemental powders [J]. Intermetallics, 2011, 19: 154−159.

[12] SCHMOELZER T, LISS K D, ZICKLER G A, WATSON I J, DROESSLER L M, WALLGRAM W, BUSLAPS T, STUDER A, CLEMENS H. Phase fractions, transition and ordering temperatures in TiAl−Nb−Mo alloys: An in- and ex-situ study [J]. Intermetallics, 2010, 18: 1544−1552.

[13] LI Shu-suo, SU Xi-kong, HAN Ya-fang, XU Xiang-jun, CHEN Guo-liang. Simulation of hot deformation of TiAl based alloy containing high Nb [J]. Intermetallics, 2005, 13: 323−328.

[14] WANG Gang, XU Lei, WANG Yong, ZHENG Zhuo, CUI Yu-you, YANG Rui. Processing maps for hot working behavior of a PM TiAl Alloy [J]. Journal of Materials Science & Technology, 2011, 27: 893−898.

[15] BAO Ying, YANG Dong-ye, LIU Na, ZHANG Guo-qing, LI Zhou, CAO Fu-yang, SUN Jian-fei. High temperature deformation behavior and processing map of hot isostatically pressed Ti−47.5Al−2Cr−2Nb−0.2W−0.2B alloy using gas atomization powders [J]. Journal of Iron & Steel Research (International), 2017, 24: 435−441.

[16] KOMMEL L, SHAHREZA B O, MIKLI V. Microstructure and physical-mechanical properties evolution of pure tantalum processed with hard cyclic viscoplastic deformation [J]. International Journal of Refractory Metals and Hard Materials, 2019, 83: 104983.

[17] PRASAD Y V R K, GEGEL H L, DORAIVELU S M. Modeling of dynamic material behavior in hot deformation: Forging of Ti-6242 [J]. Metallurgical Transactions A, 1984, 15: 1883−1892.

[18] BOZZINI B, CERRI E. Numerical reliability of hot working processing maps [J]. Materials Science & Engineering A, 2002, 328: 344−347.

[19] MA Ming, DING Hua, TANG Zheng-you, ZHAO Jing-wei, JIANG Zhou-hua. Effects of temperature and strain rate on flow behavior and microstructural evolution of super duplex stainless steel under hot deformation [J]. Journal of Iron & Steel Research (International), 2016, 23: 244−252.

[20] LI Jian-bo, LIU Yong, WANG Yan, LIU Bin, HE Yue-hui. Dynamic recrystallization behavior of an as-cast TiAl alloy during hot compression [J]. Materials Characterization, 2014, 97: 169−177.

[21] LI Jian-bo, LIU Bin, WANG Yan, TANG Shan, LIU Yong, LU Xiao-fang. A study on the Zener-Holloman parameter and fracture toughness of an Nb-particles-toughened TiAl−Nb alloy [J]. Metals, 2018, 8: 287.

[22] LI Jian-bo, LIU Yong, WANG Yan, LIU Bin, LU Bin LIANG Xiao-peng. Constitutive equation and processing map for hot compressed as-cast Ti−43Al−4Nb−1.4W−0.6B alloy [J]. Transactions of Nonferrous Metals Society of China, 2013, 23: 3383−3391.

[23] SUN Yu, WAN Zhi-peng, HU Lian-xi, REN Jun-shuai. Characterization of hot processing parameters of powder metallurgy TiAl-based alloy based on the activation energy map and processing map [J]. Materials & Design, 2015, 86: 922−932.

[24] SINGH V, MONDAL C, KUMAR A, BHATTACHARJEE P P, GHOSAL P. High temperature compressive flow behavior and associated microstructural development in a β-stabilized high Nb-containing γ-TiAl based alloy [J]. Journal of Alloys and Compounds, 2019, 788: 573−585.

[25] SHERWOOD P J, GUIU F, KIM H C, PRATT P L. Plastic anisotropy of tantalum, niobium, and molybdenum [J]. Canadian Journal of Physics, 1967, 45: 1075−1089.

[26] FENG Q, WHANG S H. Deformation of Ti−56at.%Al single crystals oriented for single slip by 1/2<110] ordinary dislocations [J]. Acta Materialia, 2000, 48: 4307−4321.

[27] ZHOU Can-xu, LIU Bin, LIU Yong, QIU Cong-zhang, LI Hui-zhong, HE Yue-hui. Effect of carbon on high temperature compressive and creep properties of β-stabilized TiAl alloy [J]. Transactions of Nonferrous Metals Society of China, 2017, 27: 2400−2405.

[28] KONG Fan-tao, CHEN Yu-yong, ZHANG De-liang, ZHANG Shu-zhi. High temperature deformation behavior of Ti−46Al−2Cr−4Nb−0.2Y alloy [J]. Materials Science & Engineering A, 2012, 539: 107−114.

Ta 颗粒增强 TiAl 复合材料的加工图及热变形行为

袁程浩，刘 彬，刘宇熙，刘 咏

中南大学 粉末冶金国家重点实验室，长沙 410083

摘 要：通过放电等离子烧结制备 Ti−48Al−2Cr−2Nb−0.2W(摩尔分数，%)/20%(体积分数)Ta 金属基复合材料。在温度 1050~ 1200 °C 及应变速率 1×10^{-3}~1 s^{-1} 的条件下，通过热压缩试验研究复合材料的变形行为。建立包含真应变变量的本构方程。不同应变下，复合材料的激活能 Q 值为 240~280 kJ/mol，低于纯 TiAl 的激活能。在动态材料模型的基础上，建立不同应变下的加工图，得到热加工最优参数为：1050~1100 °C 和 0.005~0.01 s^{-1}。研究复合材料在变形过程中的显微组织演变。结果表明，动态再结晶在变形过程中起着重要作用。

关键词：TiAl 基复合材料；流变行为；加工图；动态再结晶

(Edited by Wei-ping CHEN)